

## Applying CFD to Characterize Gear Response during Intensive Quenching Process

*Andrew Banka, Jeff Franklin*

*Airflow Sciences Corporation, 12190 Hubbard Street, Livonia, MI 48150*

*Zhichao Li, Blake L. Ferguson*

*Deformation Control Technology, Inc. 7261 Engle Road, Suite 105, Cleveland, OH 44130*

*Michael Aronov*

*IQ Technologies, Inc. Akron, Ohio 44309*

### Abstract

Steady state and transient CFD analyses using FLUENT® are applied to the intensive quenching process to characterize the water flow and thermal boundary conditions around a test gear made of carburized Pyrowear® 53. The varying transient heat transfer rates around the gear surface are predicted from CFD models and imported to heat treatment models using DANTE® to predict the gear response, including hardness, phase transformation, stress, and distortion. The relations between temperature field, phase transformation, internal stress, and distortion during quenching are explained using the modeling history results. The combination of FLUENT and DANTE models provides efficient and effective solutions to the quenching fixture and water flow designs.

### Introduction

Quenching is a fast transient thermal process. During quenching, the part is heated above the austenitization temperature, then the part is cooled rapidly by the quenching media. According to the quenchant type being used, the quenching process can be classified as liquid quenching or gas quenching. Liquid quenching includes oil quenching, water and polymer quenching, and molten salt quenching. For all the quenching processes, the quenchant flow condition has a primary effect on quenching results, including microstructural phase distribution, hardness, residual stress, and distortion. Therefore, characterization of the quenchant flow is important for understanding the quenching process. With the development of high-speed computer and computational fluid dynamics (CFD) technologies, the quenchant flow pattern during quenching can be calculated. The cooling uniformity among parts in a quenching rack has been predicted using CFD, as well as the cooling difference at different locations of a single part.[1] The oil velocity in a quench tank was predicted by static CFD analysis using FLUENT. To couple to a thermal-stress model using the finite element method, the quenchant velocities were converted to heat transfer coefficients along the part surfaces and used as thermal boundary conditions to drive a heat treatment model.[2] Part distortion due to non-uniform cooling was then predicted using DANTE.[2]

Kobasko developed intensive quenching more than 30 years ago.[3] Compared to traditional oil or water/polymer quenching, intensive quenching uses plain water or water-salt solutions as the quench media. Intensive quenching is characterized by extremely high cooling rates of steel parts. Due to the high thermal gradient and rapid surface and near-surface formation of martensite at the beginning of the process, intensive quenching can generate high compressive residual stresses in the part surface. High surface compressive residual stresses are desired in most cases to improve the fatigue life of the heat treated part. Studies have shown that intensive quenching can be applied to both carburized and non-carburized steel parts. [4-6]

During intensive quenching, high speed water flows along the surface of the part. The intent is to extract heat quickly and uniformly from the part, and vapor blanket and nucleate boiling during quenching are not desired. However, the water flow at concave locations of the part may be stagnant, which will cause a much lower cooling rate than the average. On the other hand, the cooling rate at outer corners and edges can be much higher than the average, which may cause cracking at these locations due to high thermal stresses. Fixtures for the IQ process can be designed to direct the water flow more uniformly along the surface of the part, so as to improve uniformity of cooling. In this paper, CFD predictions of the water flow field and surface heat transfer rates along a test gear are used to assess the intensive quench fixture design. The quenchant temperature and heat transfer coefficients along the gear surface are used as input to drive DANTE models to predict the metallurgical, stress and distortion responses of the gear.

### CFD Modeling

The intensive quench fixture featured in this study is designed to emphasize the cooling of the gear teeth, and the water has a radial flow pattern, as shown in Figure 1. The incoming water flows down the pipe, is diverted outward by the upper cone, and then enters the gear chamber radially. A portion of the flow travels over the gear and through the bore, while the balance flows under the gear and out.

The heat flux rate on the surface of the gear is expected to vary from location to location due to several factors, including 1) variations in the velocity in the vicinity of the gear, 2) the thickness of the velocity boundary layer, and 3) the thickness of the thermal boundary layer. Proper prediction of these effects requires a well resolved model with sufficient near surface grid points.

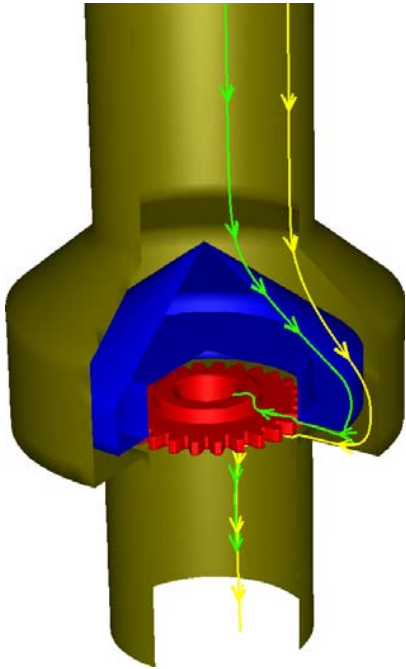


Figure 1: Cutaway view of the quench fixture showing the gear (red), upstream deflector (blue), and representative water path lines passing over and under the gear (green, yellow).

While it is expected that the heat flux rates will vary greatly with time, it is not clear that these rates will vary in the same way at different surface locations. Due to the high heat flux rates and rapid temperature changes inherent in IQ processes, the transients are expected to be brief.

While it would seem that a full, 3D, transient analysis would be necessary to fully characterize the heat flux rates throughout the process, such a simulation is currently impractical due to the computing resources that would be needed. Instead, a method is developed wherein 2D transient modeling is used to develop a characterization of the variations in heat transfer due to location and time in the quench process. That characterization is then used to predict the 3D transient heat flux rates.

All CFD simulations performed for this paper assume that boiling phenomena will be short-lived and will not have a major impact on the resulting material properties. For high velocity intensive quenching process, this assumption is reasonable.

## 2D Axisymmetric CFD Modeling

Figure 2 shows the domain and the computational grid used for the 2D gear CFD modeling. The geometry of the 2D solid used in this model is equivalent to a 3D gear blank before the teeth are hobbled. A total of 50,391 computational cells were used for this model, with 22,121 cells within the gear blank solid. The first row of cells adjacent to the gear blank is 0.05 mm thick, resulting in  $y^+$  values ranging from 20 to 300. The standard wall function model within FLUENT was used for all simulations. A total of 10 seconds of quench were simulated using a time step size of 0.001 seconds.

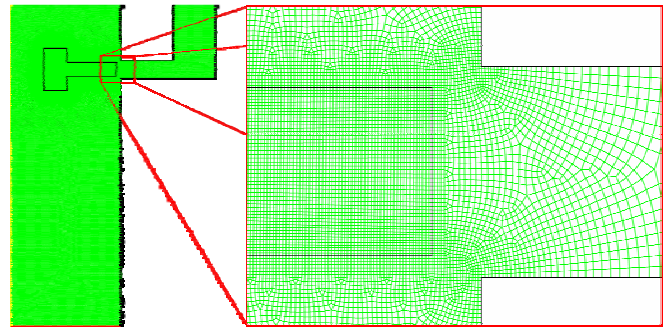


Figure 2: Domain and mesh for the 2D gear blank simulation. 50,391 total computational cells, with 22,121 cells in the solid.

The total velocity field (velocity magnitude) at the beginning of the quench is shown in Figure 3. High velocities are seen on the outside corners of the gear blank. The large faces of the gear blank see lower velocities that will result in lower heat flux rates. The tooth face of the gear blank is exposed to impinging flow, and is expected to have good heat transfer due to water temperature and flow direction even though the velocities are low. This velocity pattern remains largely unchanged throughout the duration of the quench cycle.

Figure 4 shows the time history of the heat flux at 3 points on the surface of the gear blank. These points have been chosen to highlight the behavior for regions with significantly different water flow conditions. While the initial heat flux rates differ by a factor of more than 4, all curves asymptotically approach zero at long times. Figure 5 shows the time history of the heat transfer coefficient at these three points. Again, the values vary widely both by location and by time. Thus, the assumption of a uniform heat transfer coefficient for the quenching process is unlikely to properly represent the quenching environment.

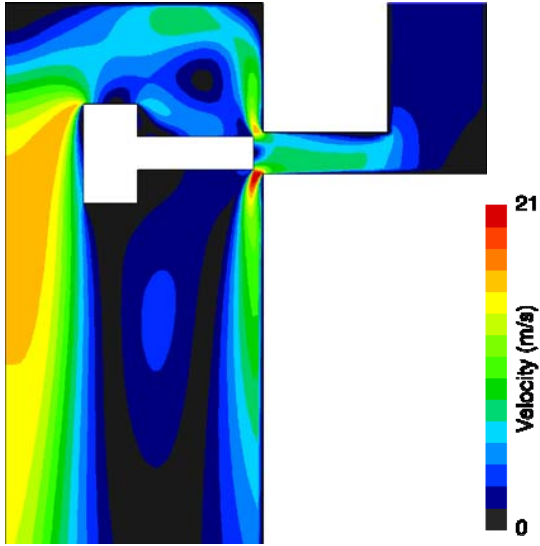


Figure 3: Total velocity plot of water flowing through quench fixture and around gear blank.

### Development of Correlation Function

As noted above, it is possible but not currently practical to perform a full 3D transient simulation of complex geometries in order to define the heat transfer rates during quenching. Nevertheless, the 2D model presented above shows that the heat flux rates and heat transfer coefficients vary considerably with time and from one location to the next. The challenge is to extract sufficient information from one or two steady-state CFD simulations to characterize the heat transfer rates over the entire quench cycle. Such a characterization is expected to provide significantly improved accuracy over current methods, in which a constant heat transfer coefficient is assumed.

Equation 1 was found to provide an accurate representation of the overall trends for the heat transfer rates on the 2D gear blank presented above. It attempts to blend steady-state simulation results obtained from hot and cold conditions in a way that largely duplicates the actual transient behavior.

$$q = \left[ h^o \frac{T_w - T_r}{T_w^o - T_r} + h^f \frac{T_w^o - T_w}{T_w^o - T_r} \right] \left( T_w - \left[ T_o \frac{T_w - T_r}{T_w^o - T_r} + T_r \frac{T_w^o - T_w}{T_w^o - T_r} \right] \right) \quad \text{eq.[1]}$$

where:

- $h^o$  is the initial local heat transfer coefficient;
- $h^f$  is the final local heat transfer coefficient (when the part is fully cooled);
- $T_w^o$  is the initial temperature of the part;
- $T_r$  is the reference fluid temperature (inlet fluid temperature);
- $T_o$  is the initial near surface characterization temperature;
- and
- $T_w$  is the current wall temperature.

Note that the local heat transfer coefficients used in equation 1 differ from those presented in Figure 5. In Figure 5, the temperature differential is between the surface and the fluid inlet temperature, while the temperature differential for the local heat transfer coefficient is between the surface and the near surface fluid temperature.

The first term in this equation provides a blending from the initial local heat transfer coefficient to the final value, while the second term provides the temperature differential, including a blending of the near surface liquid temperature from the initial to final values. Three variables in this equation are obtained from the CFD simulations.  $h^o$  and  $T_o$  are obtained from a steady-state simulation with the part surface held at its initial temperature, while  $h^f$  is obtained from a steady-state simulation with the part surface at the water inlet temperature. These values are independently found for each surface location on the gear, and later applied to the DANTE model.

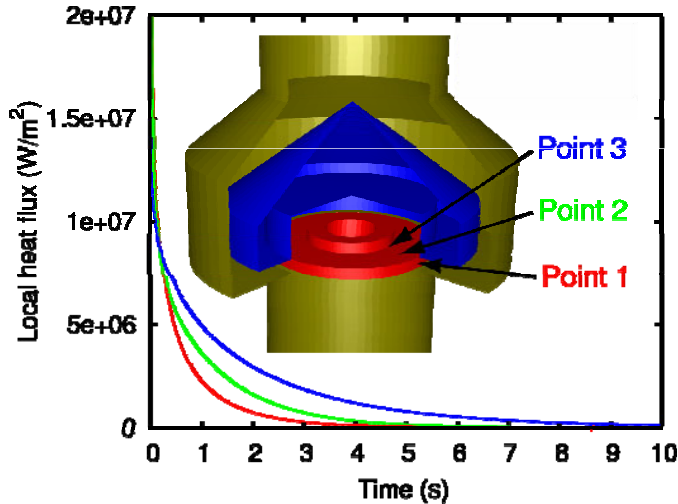


Figure 4: Time history of surface heat flux for three points on gear blank from 2D transient simulation.

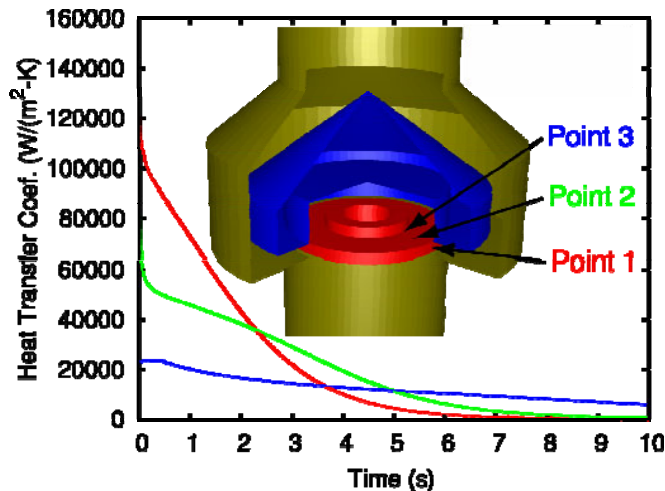


Figure 5: Time history of surface heat transfer coefficient for three points on gear blank from 2D transient simulation.

Figure 6 shows the correlation between the simulated heat flux values from the transient simulation compared to the values predicted by the equation. Very good correlation is seen for Points 1 and 2. The correlation for Point 3 is not as good, most likely due to the poor flow in this area.

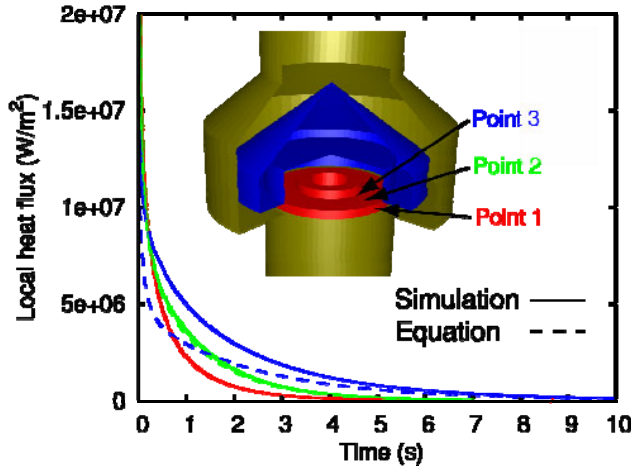


Figure 6: Comparison of simulated heat flux values and estimated values for 3 points on the 2D gear blank model.

### Steady-State 3D CFD Modeling

Figure 7 shows the grid used for the steady-state 3D CFD modeling. The inherent symmetry of the geometry was used to reduce the domain to a half gear tooth. A total of 1,721,070 computational cells were used in the model. The gear solid was not included in the model. Instead, the gear surface temperature was specified on the boundary of the fluid domain. The model was run for both the hot part surface and the ambient part surface in order to determine the  $h^0$ ,  $h^f$ , and  $T_0$  values in the equation shown before. The heat transfer coefficients are displayed in Figures 8 and 9.

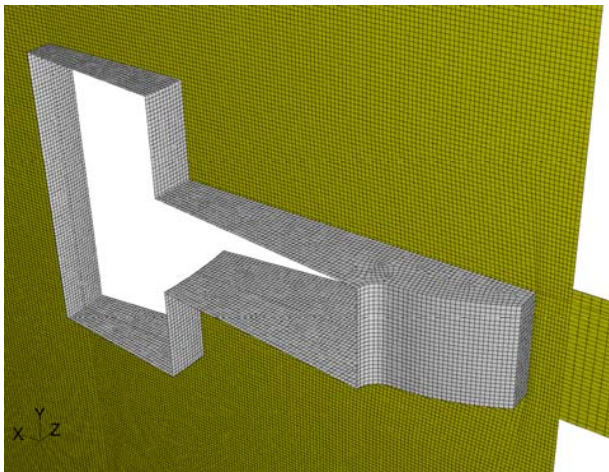


Figure 7: Computational domain and grid used for 3D gear model.

The bottom side of the gear is displayed in these figures, as those surfaces show a greater variation than the top side. As suggested in Figure 3, more of the fluid passes under the gear than over, leading to the highest heat transfer rates on the lower corner of the gear tooth. This is seen for both the initial and final local heat transfer coefficients. The characterization temperatures shown in Figure 10 depict a pattern that is largely the inverse of the heat transfer coefficients. Where the flow velocity is low, the heat transfer coefficient will be low and the low velocity will also allow the fluid to gain more heat from the part, thereby raising the local fluid temperature.

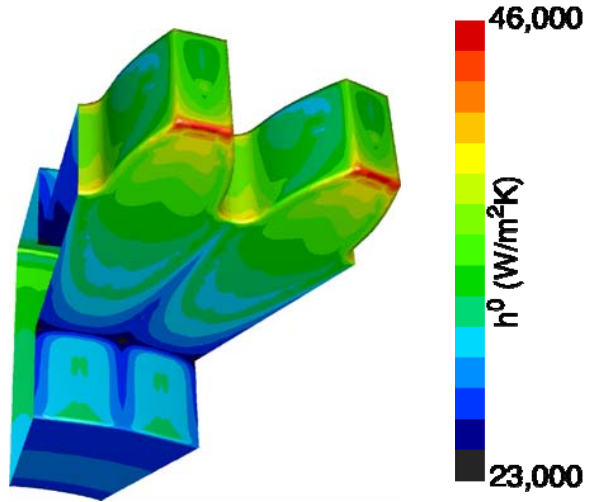


Figure 8: Initial local heat transfer coefficient values on the surface of the gear.

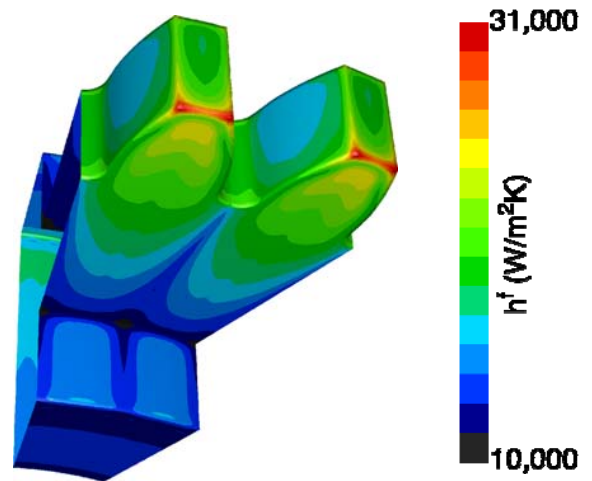


Figure 9: Final local heat transfer coefficients on the surface of the gear.

### Heat Treatment Model

In this paper, the CFD model and the heat treatment model use different meshing grids. However, the element sizes in the

heat treatment model have been limited so that the heat transfer boundary conditions reported from CFD results could be effectively applied. A single tooth finite element model was created to predict the gear response during the intensive quenching process, as shown in Figure 10. The bore diameter of the gear is 30 mm, and the tip diameter of the gear is 95.25 mm. The gear has 28 teeth in total. There are 5979 nodes and 4820 brick elements in the single tooth heat treatment model. The heat treatment process includes furnace heating, carburization, and intensive quenching. Deep freeze and tempering modeling are not included in this paper. During carburization, only the gear tooth surface is carburized, and all the other surfaces including the tip surface are copper plated. Fine elements are used in the tooth surface to catch the carbon gradient.

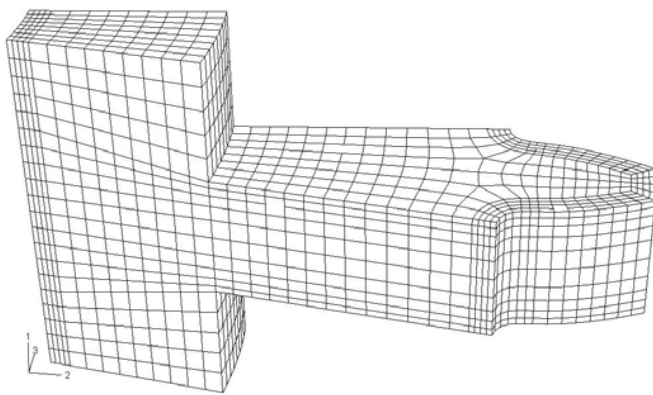


Figure 10: Finite Element Meshing for DANTE Heat Treatment Modeling

Cyclic symmetric boundary conditions are used for both the thermal and stress heat treatment models. Therefore, the responses of all the 28 gear teeth are same. This type of model cannot predict ovality and potato chip distortion. The radial and axial distortion of the gear tooth are reported.

### Modeling the Carburization Process

The gear is made of Pyrowear 53, which has a base carbon of 0.1%. The gear is gas carburized, and a brief carburization schedule is listed below:

- Carburization temperature is 926.7° C,
- Carbon potential is 0.8%,
- Carburization time period is 8 hours.

The carbon contour plot after the carburization process is shown in Figure 11(a). The surface carbon is about 0.8%. Line EF is located in the gear root around the fillet as shown in Figure 11(a). The carbon distribution in term of depth from the gear surface along line EF is shown in Figure 11(b). The case depth is about 0.6 mm.

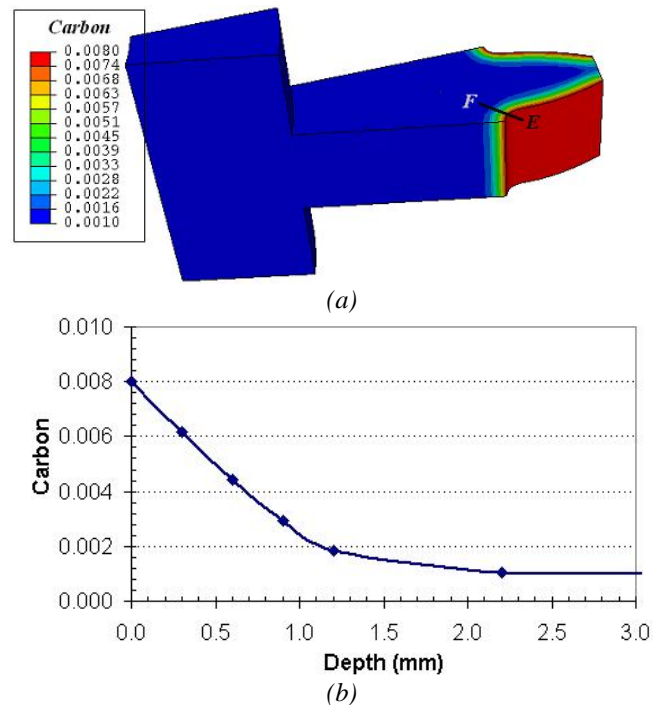


Figure 11: Carbon Distribution in terms of Weight Fraction: (a) Contour Plot; (b) Along Line EF

### Analysis of Heat Treatment Modeling Results

The correlated heat flux based on equation 1 was used as the thermal boundary conditions to drive the DANTE heat treatment model. The heat transfer coefficients and the local ambient temperatures are dependent on both the surface of the part and quenching time.

Two lines of nodes were selected to investigate the effects of temperature and phase transformations on internal stress and distortion evolution. The two lines are shown as line AB and line CD in Figure 12. Figure 12 shows half of the gear tooth cut through plane ACBD. Line AB is located at the half gear height. Both lines AB and CD are located on the half symmetry plane of the single gear tooth.

Pyrowear 53 has high hardenability due to its high alloy content. During the intensive quenching process, the only phase formed from austenite is martensite, and the sum of the volume fractions of austenite and martensite equals one. For reference, Figure 13 shows the relationship between carbon content and the martensite start temperature,  $M_s$ .

The austenitization temperature of the gear is 926.7° C. There is a 10-second air transfer time from the furnace to the quench tank. Figure 14(a) shows the temperature distributions along line AB at different quenching times. The temperature distribution at the end of the air transfer stage is shown as the

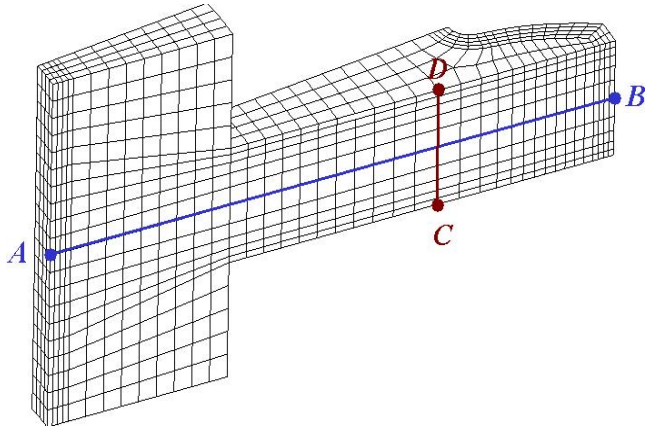


Figure 12: Lines AB and CD Selected for Heat Treatment Result Analysis

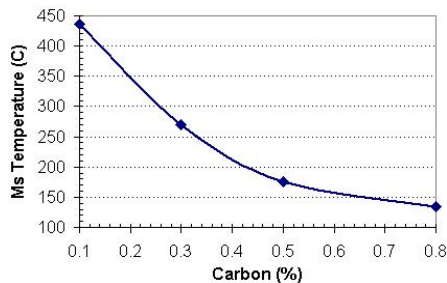


Figure 13: Effect of Carbon Content on the Start of Martensite Formation Temperature for Pyrowear 53.

line marked with 0.0 s in Figure 14(a). The temperature at point A (the bore of the gear) has dropped to about 900 ° C, and the temperature at point B (the tip of the gear) has dropped to 870° C, so the temperature at the tooth tip is 30° C lower than the temperature of the bore at the start of IQ.

During the early stages of intensive quenching, a steep thermal gradient at the part surface is quickly established due to the high rate of heat extraction. Because of the gear tooth shape, differences in local carbon contents and thus differences in local martensite formation, and the steep temperature gradients, interpretation of model results requires that temperature, metallurgical phase and stress results be examined in concert.

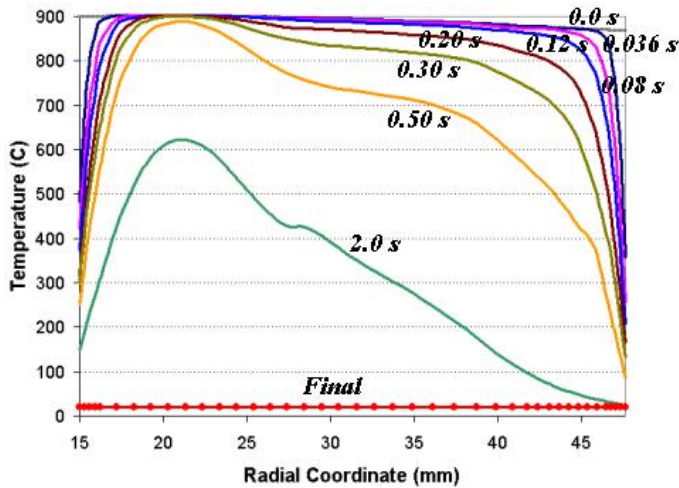
In Figure 14, the radial coordinates of the line AB shown in Figure 12 form the X axis. The centerline of the gear has a radial coordinate of zero. Figure 14(b) shows the austenite distribution along line AB at indicated quenching times. The martensitic transformation starts at the tip surface at a time between 0.08 and 0.12 seconds. The transformation in the low carbon tip surface is nearly done after about 0.5 seconds quenching. Compared to traditional oil quenching, the cooling rate for intensive quenching is much higher.

During quenching of steel parts, the thermal gradient and phase transformations are the two main contributions to the

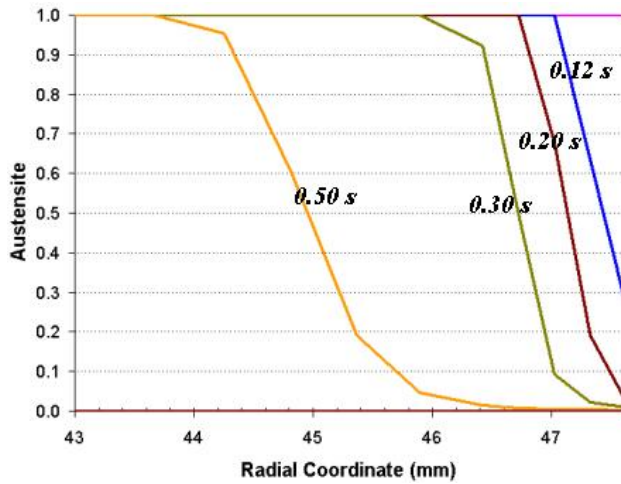
internal stress evolutions. Figure 14(c) shows the hoop stress along line AB at indicated quenching times. The stress in the gear after austenization is sufficiently low that it can be assumed to be stress free. The carburization process introduces a slight compressive stress in the carburized gear surface. During the 10-second air transfer time from furnace to quench tank, the temperatures of the gear tooth surface (carburized) and gear tip surface drop. The temperature decrease at the gear tip surface causes the thermal contraction, which tends to introduce tensile stress to point B. On the other hand, the temperature decrease at the carburized gear tooth surface imposes a compressive stress at point B due to a geometry effect. This combined effect generates a compressive hoop stress of 45 MPa at point B, as shown by 0.0 s line in Figure 14 (c).

At 0.036 seconds during intensive quenching, a tensile hoop stress of 170 MPa is predicted at point B purely due to greater thermal contraction of the cooler surface as compared to the hotter subsurface. No phase transformation has occurred at this time. As the surface continues to rapidly cool, higher surface tension leads to local plastic deformation of the surface in the early quenching stage due to the high thermal gradient. This is one key to the final residual stress generated in this carburized part. At 0.08 second, the cooling rate at the subsurface exceeds the cooling rate at the surface since the surface is nearly at the water temperature. The surface tensile hoop stress drops from 170 MPa to 105 MPa at the end of 0.08 seconds of quenching. As shown in Figure 14(b), the martensitic transformation starts between 0.08 second and 0.12 second at point B. During this time period, the phase transformation rate on the tooth tip surface is higher than that of the subsurface. Due to the material expansion caused by martensitic transformation, the point B on the tip surface shows 320 MPa hoop stress in compression at the end of 0.12 second quenching. To balance the surface compressive stress, a tensile stress peak of 150 MPa is observed at the depth of about 0.5 mm from the tip surface, which matches the transformation interface, as shown by the 0.12 s line in Figure 14(b) and (c). Note well, the line AB does not traverse through the carburized case so the carbon content is constant at the baseline level along this line. At this time, no martensite has begun to form in the carburized case.

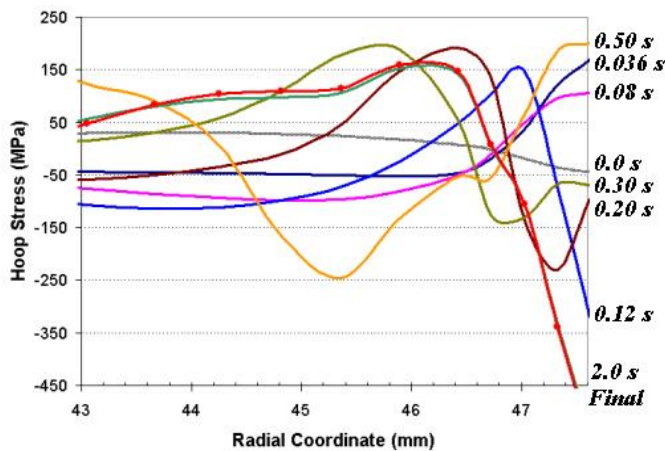
With longer quenching time, the phase transformation interface moves inward from the tip surface. Between 0.12 and 0.2 seconds, the phase transformation rate in the subsurface exceeds the transformation rate on the surface. As shown by the 0.2 s line in Figure 14(c), the tensile stress peak also moves inward. A compressive stress peak is observed at the shallow depth from the tip surface; this is the location which has the highest martensitic transformation rate. From 0.2 to 0.3 seconds during intensive quenching, both the tensile and compressive stress peaks move inward from the tip, and the level of tip surface compression is reduced. At 0.5 second, the highest transformation rate occurs at the depth of 2.2 mm from the tip surface, as shown by the 0.5 s line in Figure 14(b). The compressive stress peak is about 150 MPa, as



(a)



(b)



(c)

Figure 14: Temperature and Phase Transformation Histories Along Line AB from DANTE Simulation Results: (a) Temperature History; (b) Phase Transformation History; (c) Internal Stress Evolution

shown in Figure 14(c). The depth of the tensile stress peak at 0.5 second is about 6.0 mm from the tip surface, and the hoop stress value is 200 MPa in tension. Due to the combined effect of the thermal gradient and martensitic phase transformations, the hoop stress at point B (the gear tip surface) is about 200 MPa in tension at the end of 0.5 second in quenching.

The intensive quenching is essentially completed in about 2.0 seconds for this specific gear and gear steel. At the end of quenching, a compressive hoop stress of 550 MPa is predicted at point B (gear tip surface). Finite element analysis shows that both thermal gradient and phase transformations are very important to the stress evolution during quenching. Plastic deformation of austenite under tension during quenching is also key to the final residual stress distribution.

The main purpose of applying CFD analysis results to the finite element model of the intensive quenching process is to accurately characterize the nonuniform thermal boundary conditions. Knowledge of the water flow pattern, the local velocity, and the quenchant ambient temperature along the gear surface is required for assigning meaningful heat transfer coefficients along the surface of the gear during the heat treatment analysis. Without CFD results, the assumed heat transfer boundary conditions have been constant and uniform conditions. Because the gear is symmetric to the plane ABCD and normal to the gear axis, for these assumed conditions, line AB always remains straight and parallel to the X-axis during the FEA analysis. With these assumed uniform thermal boundary condition on the gear, FEA analysis cannot predict warping distortion, which is shown in Figure 14(c) by the line with hollow round marks. The ability to predict nonuniform heat transfer conditions due to nonuniform quenchant flow is an important aspect of CFD analysis.

Nodes on line CD in Figure 12 are selected to investigate how potential warping distortion is generated during intensive quenching. CFD analysis shows that the top and bottom surfaces of the gear hub cool differently during quenching. In Figure 15(a) and (b), the X-axis matches the nodal positions of line CD in Figure 12 with point C locating on the left side of the X-axis and D to the right. Point X=0 is located at the midpoint of the line CD. In Table 1,  $\Delta T$  is the temperature difference between point C and point D at different quenching times. Warping distortion of the gear is defined as the difference of axial displacements at point A and point B at difference quenching times.

There is no phase transformation occurring along line CD before 0.036s seconds of intensive quenching, so the thermal gradient is the only cause of warping at this stage. At 0.036 seconds of quenching, the temperature at point C is about 425° C, and the temperature at point D is about 535° C. The temperature difference is 110° C, as listed in Table 1. Greater thermal contraction at point C leads to warping of 0.032 mm downward. At 0.08 seconds, the temperature difference between points C and D increases, and only a small amount of

phase transformation occurs on the bottom hub surface. As a result, the warping distortion increases to 0.051 mm downward. At 0.12 seconds, the temperature difference between points *C* and *D* has increased to 147° C. The increased temperature difference increases the warping distortion in the downward direction. However, the temperature on the bottom of the hub (point *C*) is well below the martensitic transformation starting temperature. Martensitic phase transformation in the bottom surface causes material volume expansion, which compensates the downward warping due to temperature difference alone. As shown by the 0.12 s line in Figure 15(c), the direction of warping starts to reverse. With longer time in quenching, the temperature difference between top surface and bottom surface decreases, and both top and bottom surfaces transform to martensite. The final warping distortion is about 0.24 mm in an upward direction.

Table 1: Relation of temperature difference and bow distortion

Quenching Time (s)	0.036	0.08	0.12	0.2	0.3	0.5	2.0	Final
$\Delta T$ (°C)	110	121	147	109	108	97	39	0.0
Bowing (mm)	-0.032	-0.051	-0.027	0.007	0.041	0.105	0.203	0.24

### Summary and Conclusions

The prediction of heat flux rates for a quenched part using CFD analyses ideally requires a finely resolved grid and a transient solution. The combination of high resolution and time dependence makes such simulations impractical for complex 3D shapes, even with today’s current computing technology. In order to overcome this problem, a method has been developed to provide a very good characterization of the transient heat flux behavior from two steady-state simulations. This approach was developed using a 2D gear blank model to simulate the intensive quenching process using a full, transient CFD analysis. A bridge between the transient CFD analysis and steady-state CFD analyses was then built. Simulation results show that it is practical to represent the transient analysis by interpolating two steady-state CFD analyses.

Two 3D steady-state CFD analyses were then done using a half single tooth model. By applying the interpolation equation developed above, a transient heat transfer boundary condition for the 3D gear tooth was defined for use in a subsequent heat treatment model.

By using the CFD results as a driver, a 3D single gear tooth model was developed and simulated using DANTE. The relationships among the temperature, phase transformation, internal stresses, and distortion were addressed. The simulation results showed that the cooling rate during intensive quenching was very high, as expected. The high rate of localized heat extraction and the short times for quenching

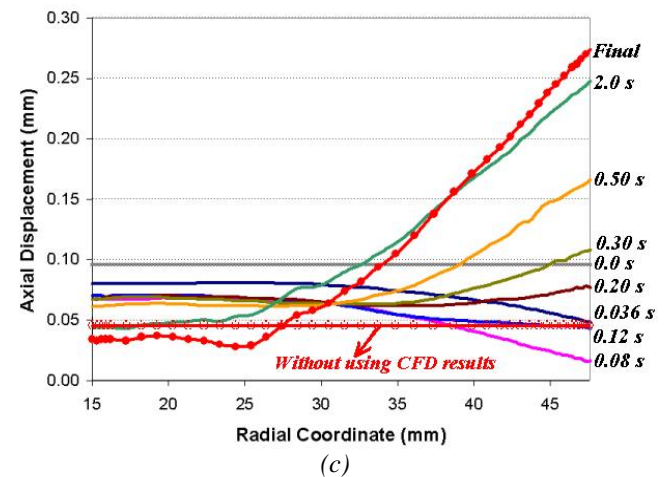
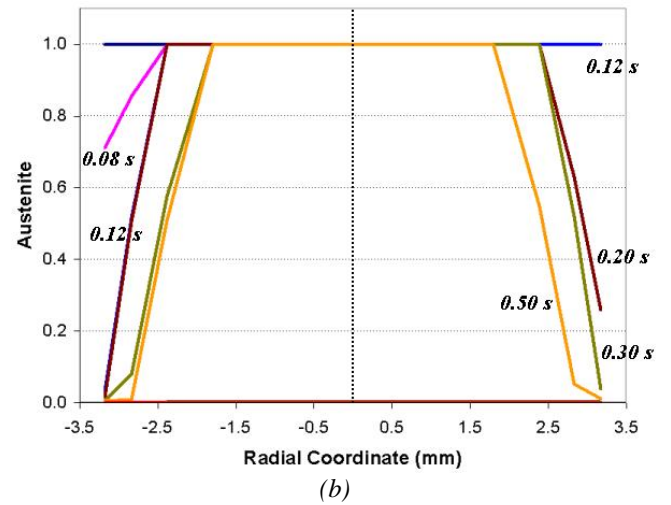
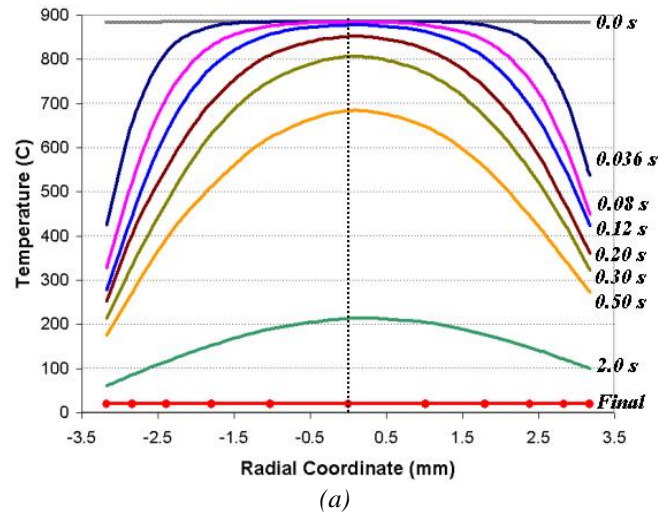


Figure 15: Generation of Warping Distortion: (a) Temperature History along Line CD; (b) Phase Transformation History along Line CD; (c) Displacement History along Line AB

and phase transformation make the process sensitive to issues of timing, and to uniformity, direction, and magnitude of quenchant flow, and establishes the need for the process to be well controlled. The results using the CFD heat flux rates were shown to be considerably different than if a constant and uniform heat transfer coefficient was assumed.

The results presented in this paper show that the quenchant flow field can have a significant effect on the phase transformation, internal stresses, and distortion of the finished part. The combination of FLUENT CFD and DANTE heat treatment models can be effectively used in future studies to develop quench fixtures and processes that have improved uniformity of heat transfer, more desirable residual stress levels, and reduced distortion.

### Acknowledgements

Research was sponsored by the U.S. Army Benet Laboratories and was accomplished under Cooperative Agreement Number W15QKN-06-R-0501 between the Edison Materials Technology Center of Dayton, Ohio, and the U.S. Army. The views and conclusions contained in this document are those of the authors and should not be interpreted as representing the official policies, either expressed or implied, of the U.S. Army Benet Laboratories or the U.S. Government. The U.S. Government is authorized to reproduce and distribute reprints for Government purposes notwithstanding any copyright notation hereon.

### References

1. D. S. MacKenzie, A. Kumar, and H. Metwally, "Optimizing Agitation and Quench Uniformity using CFD", Proceedings of the 23<sup>rd</sup> ASM Heat Treating Society Conference, 271-278, (2005)
2. D. S. MacKenzie, Z. Li, B. L. Ferguson, "Effect of Quenchant Flow on the Distortion of Carburized Automotive Pinion Gears", 5<sup>th</sup> International Conference on Heat Treatment: Quenching and Control of Distortion, 119-129, (2007)
3. N.I. Kobasko and N.I. Prokhorenko, "Quenching Cooling Rate Effect on Crack Formation of 45 Steel," *Metallovedenie and Termicheskaya Obrabotka Metallov* (in Russian), 53-54, 2(1964)
4. M.A. Aronov, N.I. Kobasko, J.A. Powell, J.F. Wallace, and D. Schwam, "Practical Application of the Intensive Quenching Technology for Steel Parts," *Industrial Heating Magazine*, 59-63, April (1999)
5. B. L. Ferguson, A. Freborg, and Z. Li, "Residual Stress and Heat Treatment- Process Design for Bending Fatigue Strength Improvement of Carburized Aerospace Gears", 5<sup>th</sup> International Conference on Heat Treatment: Quenching and Control of Distortion, 95-104, (2007)

6. C. Hubbard, F. Tang, "Effect of Intensive Quenching on Residual Stress", Proceeding of the 23<sup>rd</sup> ASM Heat Treating society Conference, 338-342, (2005)